Available online at www.sciencedirect.com
ScienceDirect
Journal of Nuclear Materials 372 (2008) 304–311
journal of nuclear materials
www.elsevier.com/locate/jnucmat

Microstructure and corrosion characteristics of Zr–1.5Nb–0.4Sn–0.2Fe–0.1Cr alloy with a β-annealing

Hyun-Gil Kim [a,*], Jong-Hyuk Baek [a], Sun-Doo Kim [b], Young-Hwan Jeong [a]

[a] *Advanced Core Materials LAB, KAERI, 150 Doekjin-dong, Yuseong-gu, Daejeon 305-353, Republic of Korea*
[b] *Korea Nuclear Fuel Co., Ltd., Daejeon 305-353, Republic of Korea*

Received 11 August 2006; accepted 6 March 2007

Abstract

The corrosion characteristics of Zr-based alloys are very sensitive to their microstructures which are determined by the β-annealing conditions. Specimens of Zr–1.5Nb–0.4Sn–0.2Fe–0.1Cr alloy were investigated in order to obtain their optimized β-annealing conditions such as the β-annealing temperature and the cooling rate from the β-region. From the microstructural analysis, the prior β-grain size of this alloy was increased by increasing the β-annealing temperature. The martensitic structure was formed by a fast cooling rate of a water quenching from a range of 960–1200 °C and the Widmanstätten structure was formed by a slow cooling rate of an air cooling from 1050 °C. The corrosion behavior of the Zr–1.5Nb–0.4Sn–0.2Fe–0.1Cr alloy was not affected by the β-annealing temperature but it was changed by the cooling rate. The increased corrosion resistance was caused by a decreased the supersaturated Nb content in the matrix by a formation of the β-Zr phase. However, the formation of the β-Zr phase is not recommended in the β-solution annealing procedure of Nb-containing Zr-based alloy, because the aim of the β-solution annealing is to obtain a good homogeneity.

1. Introduction

The corrosion resistance of fuel claddings has been considered to be one of the important properties to control the performance and the safety of a nuclear reactor. Zr-based alloy such as Zircaloy-4 has been used as fuel cladding materials for the last few decades. Since, the corrosion of fuel claddings is the most critical issue in a high burn-up operating condition in PWRs, the development of an advanced Zr-based fuel cladding with an improved corrosion resistance was necessary. For the development of advanced cladding materials, many researches have been implemented to improve the corrosion resistance of the Zr-based alloys [1–3]. They have reported that the corrosion kinetics of Zr alloy were affected by the alloying element and the precipitates that are formed by various alloying elements. Since the combination of an alloying element such as Nb, Sn, Fe, Cr etc., is very important factor to obtain good corrosion properties in fuel cladding alloys, many researchers have tried to establish the ideal alloying elements and compositions [3,4]. It has been reported that the corrosion properties of the Nb-containing Zr-based alloys were very sensitive to certain factors such as the Nb-content and the second phase characteristics, which could be controlled by heat-treatment [1,3]. The corrosion resistance of Zr alloy was increased by the addition of Fe up to 0.2 wt% [5], and that of Zr alloy was decreased by increasing the Sn content, however, the mechanical properties of Zr alloy were increased by increasing the Sn content [6]. At KAERI, many of the Zr alloys, which were systematically controlled by an alloying element, were then tested for various properties such as their corrosion, tensile, creep, and high temperature oxidation. Therefore, a high Nb-containing Zr-based alloy was designed and its composition is Zr–1.5Nb–0.4Sn–0.2Fe–0.1Cr in wt%.

In the new alloy system, the optimum manufacturing process was one of the important factors to increase the

* Corresponding author. Tel.: +82 42 868 2522; fax: +82 42 862 0432.
E-mail address: hgkim@kaeri.re.kr (H.-G. Kim).

0022-3115/$ - see front matter © 2007 Elsevier B.V. All rights reserved.
doi:10.1016/j.jnucmat.2007.03.259

properties of the alloy. The manufacturing processes such as a β-heat-treatment temperature, the cooling rate from the β-region, and the intermediate annealing condition which is described as a ΣA parameter have been studied for commercial Zircaloy for a long time. It is necessary to setup the optimum manufacturing process for the new alloy, since Nb content of the new alloy was high. Therefore, the purpose of this investigation is to obtain the optimized β-annealing conditions for the Zr–1.5Nb–0.4Sn–0.2Fe–0.1Cr alloy.

2. Experimental procedure

Zr–1.5Nb–0.4Sn–0.2Fe–0.1Cr alloy was manufactured by a sequence of four vacuum arc re-meltings to promote the homogeneity of the alloying elements. To study the β-annealing temperature effect, a button of the melted Zr–1.5Nb–0.4Sn–0.2Fe–0.1Cr alloy was quenched from the β-regions of 960, 1050, and 1200 °C for 30 min. And to study the cooling rate effect, another button of this alloy was also applied to a different cooling rate for a water quenching and air cooling from the β-region of 1050 °C for 30 min. The cooling rate of the water quenching was about 1000 °C/s and that of the air cooling was about 4 °C/s. Therefore, Zr–1.5Nb–0.4Sn–0.2Fe–0.1Cr alloys with different β-annealing conditions were manufactured.

The microstructure evaluation by the annealing temperature was observed using an optical microscope with a polarized light. The microstructural characteristics of the alloys with different annealing conditions were analyzed by using a transmission electron microscope equipped with energy dispersive spectra. Specimens for the TEM observation were prepared using a twin-jet polishing with a solution of C_2H_5OH (90 vol.%) and $HClO_3$ (10 vol.%) after a mechanical thinning of the specimens to about 70 μm.

The corrosion test was performed in a static autoclave of 400 °C steam under a saturated pressure of 10.3 MPa. Corrosion testing specimens of 15 mm × 25 mm × 1 mm in size were cut from the annealed samples and mechanically ground with 1200 grit SiC paper. Also, the ground specimens for the corrosion test were pickled in a solution of H_2O (40 vol.%), HNO_3 (30 vol.%), HCl (25 vol.%) and HF (5 vol.%). The corrosion resistance was evaluated by measuring the weight gain of the corroded samples after suspending the corrosion test at a periodic term. To observe the oxide characteristics, a transmitted optical microscope observation and a cross-sectional TEM examination were performed on the thin oxide samples. A cross-sectional observation of the oxide sample for transmitted optical microscopy was prepared by mechanical thinning to a thickness of less than 15 μm by using a MultiPrep polishing system and that of the oxide sample for TEM was followed by ion milling process by using a Fishione 1010 model.

3. Results and discussion

3.1. Microstructural characteristics of the Zr–1.5Nb–0.4Sn–0.2Fe–0.1Cr alloy with the β-annealing conditions

A microstructural characterization study was performed to evaluate the grain shape and second phase particles in the specimens manufactured with the β-annealing temperatures of 960, 1050, 1200 °C and the cooling rate from the β-region of 1050 °C, since it is well known that the corrosion properties of Nb-containing Zr alloys are highly dependent on the microstructural characteristics of the alloys [3].

Fig. 1 shows the macroscopic microstructure of the Zr–1.5Nb–0.4Sn–0.2Fe–0.1Cr alloy with different cooling rates for a water quenching and air cooling from the β-region of 1050 °C determined by optical microscope. It was observed that the grain size of the β-phase was increased by increasing the β-annealing temperature from 960 to 1200 °C, however, the grain size of the prior β-phase was not changed with the different cooling rates. This implies that the prior β-grain size was determined by the annealing temperature

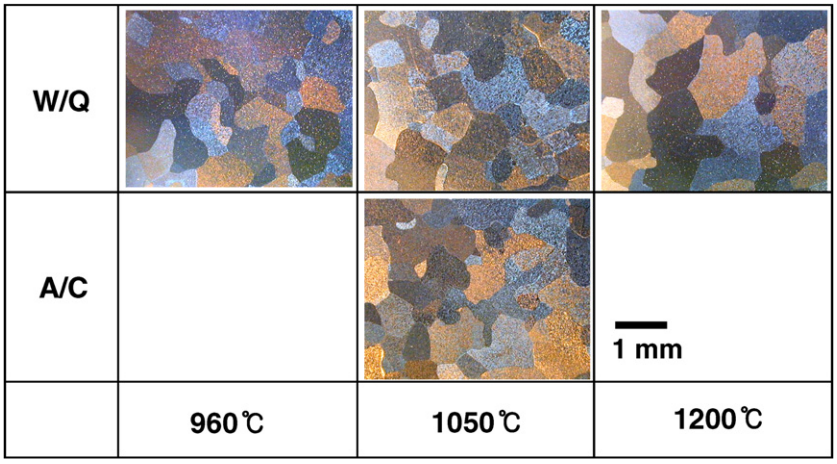

Fig. 1. Optical microstructures of the Zr–1.5Nb–0.4Sn–0.2Fe–0.1Cr alloy with different annealing temperatures and cooling rates from the β-region.

Table 1
Analyzed chemical compositions of the alloy used in this study (in wt%)

Alloy	Nb	Sn	Fe	Cr	O	C	Zr
Zr–1.5Nb–0.4Sn–0.2Fe–0.1Cr	1.48	0.38	0.21	0.10	0.135	0.012	Bal.

Table 2
Prior β-grain size of the Zr–1.5Nb–0.4Sn–0.2Fe–0.1Cr alloy with different annealing temperatures and cooling conditions

Condition	Water quenching			Air cooling
	at 960 °C	at 1050 °C	at 1200 °C	at 1050 °C
Prior β-grain size	0.99	1.02	1.07	1.03

of the β-region. The results of the prior β-grain size of the Zr–1.5Nb–0.4Sn–0.2Fe–0.1Cr alloy are shown in Table 1. The measured grain size ranged from 0.99 to 1.07 mm depending on the annealed temperature. Since, the grain size was determined by the diffusion rate of the temperature of the β-region, it was assumed that the prior β-grain size of the Zr–1.5Nb–0.4Sn–0.2Fe–0.1Cr alloy was not controlled by the cooling rates from the β-annealing temperature shown in Table 2.

It is well known that a martensite structure [7–14] is formed by a fast cooling rate and the Widmanstätten structure [15] is formed by a slow cooling rate at the β-region of the Zr alloys. Fig. 2 shows the TEM micrographs of the water quenched and air cooled Zr–1.5Nb–0.4Sn–0.2Fe–0.1Cr alloy at different annealing temperatures from 960 to 1200 °C. The martensite structure, which was mixed with dislocations and twins, was formed on the fast cooled Zr–1.5Nb–0.4Sn–0.2Fe–0.1Cr alloy regardless of the β-annealing temperature range of 960–1200 °C and the Widmanstätten structure, which was mixed with an elongated α-grain and β-phase was formed on the slow cooled Zr–1.5Nb–0.4Sn–0.2Fe–0.1Cr alloy.

In the fast cooled condition, the α-grain was not observed in the OM and TEM micrographs of the Zr–1.5Nb–0.4Sn–0.2Fe–0.1Cr alloy, although the lowest β-annealing temperature was performed at 960 °C. Therefore, it was though that the α + β to β transition temperature of the Zr–1.5Nb–0.4Sn–0.2Fe–0.1Cr alloy was lower than 960 °C. Generally, the α + β to β transus temperature of Zircaloy-4 is known to be about 970 °C [16]. The decrease of the α + β to β transus temperature in the Zr–1.5Nb–0.4Sn–0.2Fe–0.1Cr alloy compared to Zircaloy-4 is caused by Nb as an alloying element, because Nb is one of the β-stabilizing elements. And the second phase particles were not observed in the martensite structure of that alloy, therefore, the alloying elements such as Nb, Sn, Fe, and Cr were supersaturated in the martensite structure, which was formed by a water quenching at the β-region.

In the slow cooled condition, the Widmanstätten structure which was described as a basketweave structure from a previous definition [15] was observed in the air cooled Zr–1.5Nb–0.4Sn–0.2Fe–0.1Cr alloy. It is difficult to establish the microstructural differences between the water quenched and air cooled structure of this alloy from the macroscopic observation by using the OM. From the TEM observation of the Widmanstätten structure formed in the air cooled Zr–1.5Nb–0.4Sn–0.2Fe–0.1Cr alloy, a lamellar structure consisting of the α-phase and β-phase was observed in the matrix. The formation of the β-phase was affected by the contents of the alloying elements such as Nb, Fe, and Cr which act as β-stabilizers [17].

Fig. 3 shows the twined microstructure of the water quenched Zr–1.5Nb–0.4Sn–0.2Fe–0.1Cr alloy from the

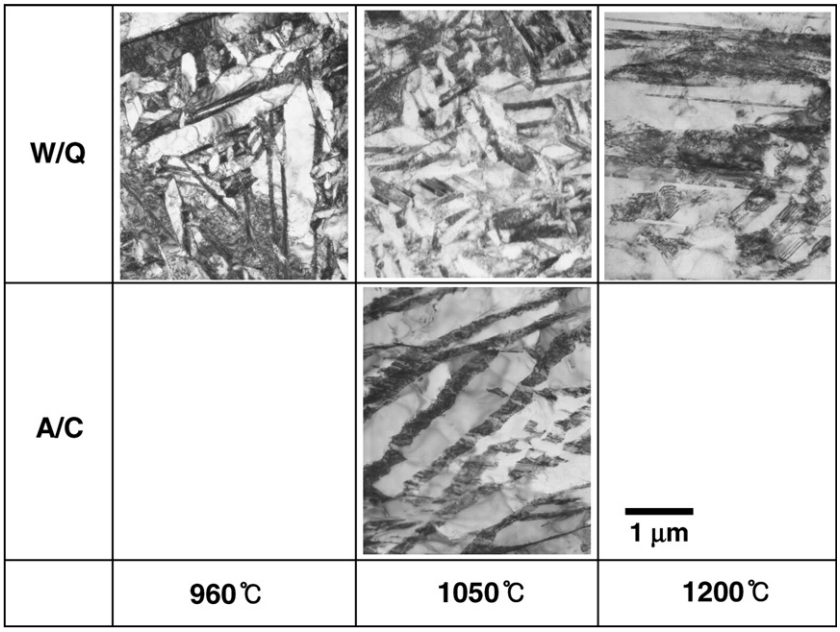

Fig. 2. TEM micrographs of the Zr–1.5Nb–0.4Sn–0.2Fe–0.1Cr alloy with different annealing temperatures and cooling rates from the β-region.

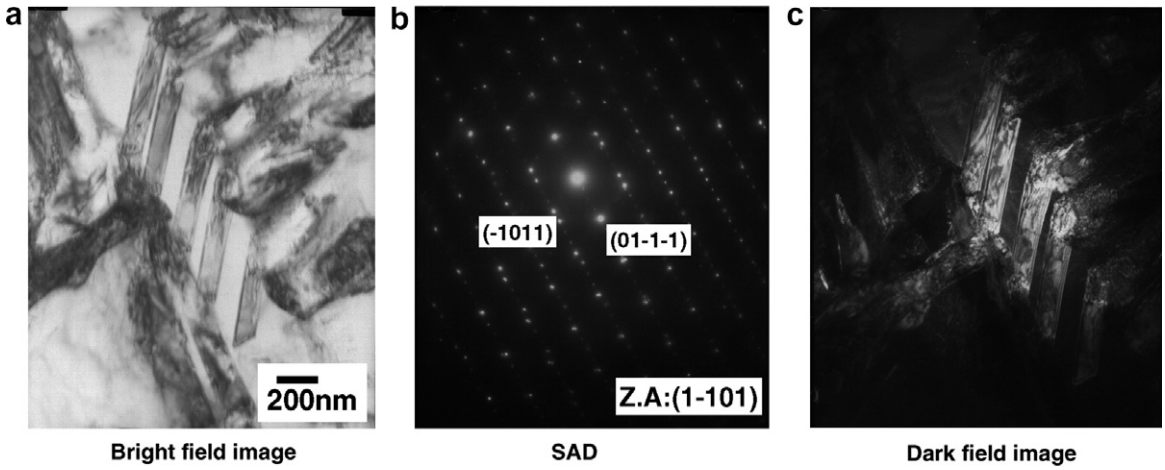

Fig. 3. TEM micrographs of the water quenched Zr–1.5Nb–0.4Sn–0.2Fe–0.1Cr alloy at the β-region of 1050 °C.

β-region of 1050 °C. The size of the twin was measured ad 500–1000 nm in length and 100–200 nm in width and dislocations were observed in the small thin twin structures which could be analyzed from the SAD and conformed from the dark field image. The common plane of the twin was revealed as $\{10\bar{1}0\}$, which is a typical twin common plane observed in zirconium alloys [14]. Hence, the microstructural characteristics of the quenched structure of the Zr–1.5Nb–0.4Sn–0.2Fe–0.1Cr alloy were quite similar to those of the quenched structure of the Zr-based alloys. Fig. 4 shows the TEM micrographs to analyze the β-phase formed on the air cooled Zr–1.5Nb–0.4Sn–0.2Fe–0.1Cr alloy from the β-region of 1050 °C. In Fig. 4(a), a lamellar structure mixed with the α- and β-phases were observed and the area fraction of the β-phase was smaller than that of the α-phase. The crystal structure of the β-phase was identified as BCC from the SAD analysis shown in Fig. 4(b). From the compositional characteristics analyzed by EDS, the β-phase formed in the Zr–1.5Nb–0.4Sn–0.2Fe–0.1Cr alloy consisted of Zr (78.4 at.%), Nb (17.6 at.%), Fe (3.1 at.%), and Cr (0.9 at.%). It could not observe for the Nb, Fe, Cr rich second phase particles in the α-Zr phase. The alloying elements of Nb, Fe, and Cr were contained in the β-Zr phase which was formed in slow cooled Zr–1.5Nb–0.4Sn–0.2Fe–0.1Cr alloy from 1050 °C.

The β-phase formation resulted in the alloying elements which were supersaturated in the β-region, being diffused into the α-phase boundary during the Widmanstätten transformation. The Nb effect of a β-phase formation of the Zr–Nb alloys with the cooling rate and the crystallographic relation between the α-phase and the β-phase have been reported [18]. From the microstructural observation of the Zr–1.5Nb–0.4Sn–0.2Fe–0.1Cr alloy with different cooling rates, the martensite structure was formed by a fast cooling, which was obtained by a water quenching from the β-phase region and the Widmanstätten structure, was formed by a slow cooling, which was obtained by an air cooling from the β-phase region. In the martensite structure, the alloying elements of the Zr–1.5Nb–0.4Sn–0.2Fe–0.1Cr alloy were supersaturated in the matrix, whereas they were diffused into the β-phase, which was identified as β-Zr in the Widmanstätten structure.

3.2. Corrosion behavior of the Zr–1.5Nb–0.4Sn–0.2Fe–0.1Cr alloy with the β-annealing conditions

Fig. 5 shows the corrosion behavior of the β-annealed Zr–1.5Nb–0.4Sn–0.2Fe–0.1Cr alloy corroded in a static autoclave with a 400 °C steam condition for up to 90 days. Generally, the exposure time steps in weight gain of Zr-based alloys are 15 or 30 days at periodic terms. In this case, the transition behavior was observed in all of the Zr-based alloys and also the weight gain range at the transition point was about 30–40 mg/dm^2. However, in the β heat treated Zr-based alloys containing high Nb, the transition behavior is unclear. Because those alloys have very high corrosion rate, therefore, it is difficulty to find the transition point during long term periodic corrosion tests. Also, it is well known that the corrosion resistance of zirconium alloys is affected by the addition of Nb as an alloying element [19–21], especially, it is considerably affected by the microstructural characteristics which are determined by the heat-treatment condition. Since, 1.5 wt% Nb was contained in the tested alloy, it was assumed that the corrosion characteristics of the Zr–1.5Nb–0.4Sn–0.2Fe–0.1Cr alloy was considerably affected by the heat-treatment conditions.

From the view point of the β-annealing temperatures of 960, 1050, 1200 °C, the weight gain of the water quenched Zr–1.5Nb–0.4Sn–0.2Fe–0.1Cr alloy reached about 450 mg/dm^2 at the corrosion test time of 90 days. Since an effect of the β-annealing temperature was not observed in the Zr–1.5Nb–0.4Sn–0.2Fe–0.1Cr alloy, the corrosion resistance of the water quenched that alloy was not affected by the β-annealing temperatures.

From the view point of the cooling rate effect, the corrosion resistance of the air cooled Zr–1.5Nb–0.4Sn–0.2Fe–0.1Cr alloy from the β-region of 1050 °C increases when compared to that of the water quenched alloy from the

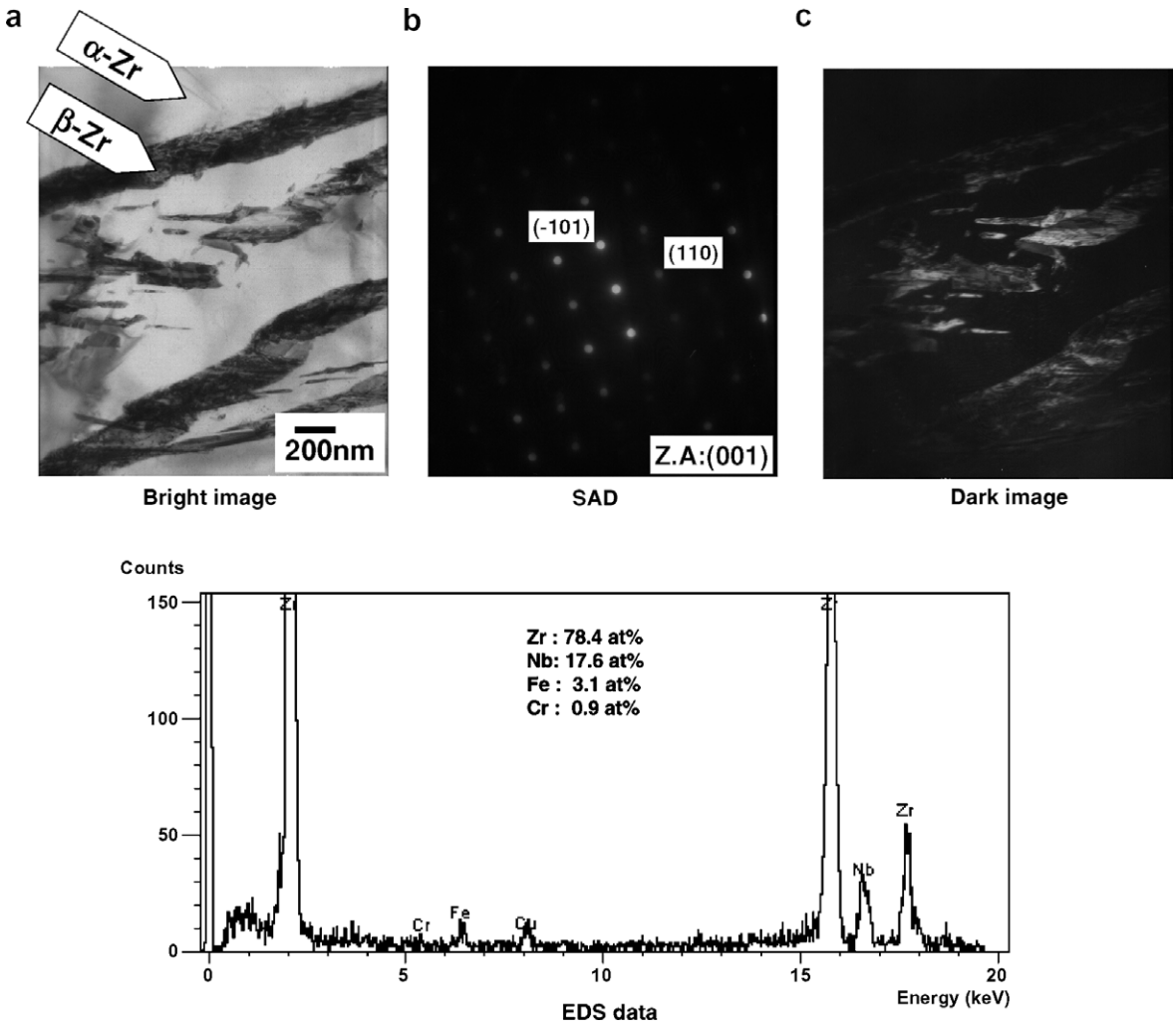

Fig. 4. TEM micrographs of the air cooled Zr–1.5Nb–0.4Sn–0.2Fe–0.1Cr alloy at the β-region of 1050 °C.

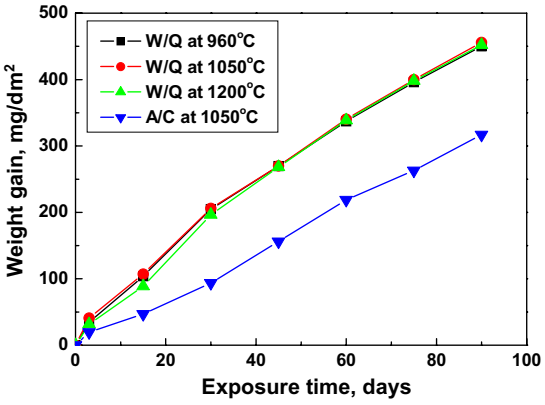

Fig. 5. Corrosion behavior of the Zr–1.5Nb–0.4Sn–0.2Fe–0.1Cr alloy with different β-annealing temperatures and cooling rates.

β-region of 1050 °C. Therefore, the corrosion resistance increases when the β-Zr phase in the matrix of the Zr–1.5Nb–0.4Sn–0.2Fe–0.1Cr alloy formed by a slow cooling. This increment of the corrosion resistance was caused by a decrement of the supersaturated Nb content in the matrix by a formation of the β-Zr phase which was defined by the TEM/EDS observation.

Since the corrosion resistance was considerably changed by the cooling rate, a microstructure observation of the cross-sectional oxide was performed for two conditions with different cooling rates. Fig. 6 shows the cross-sectional optical micrographs of the oxides of the water quenched and air cooled Zr–1.5Nb–0.4Sn–0.2Fe–0.1Cr alloy which were corroded for 60 days. The oxide thickness and the roughness of the metal/oxide interfaces were clearly defined by the cross-sectional optical micrographs. The oxide thickness of the water quenched and air cooled Zr–1.5Nb–0.4Sn–0.2Fe–0.1Cr alloy matched well with the weight gain of the corrosion data of 60 days. The roughness of the metal/oxide interfaces was shown differently with the cooling rates of the Zr–1.5Nb–0.4Sn–0.2Fe–0.1Cr alloy. In general, the uniform roughness of the metal/oxide interfaces was formed in the good corrosion resistance alloy, however, the oxide formed in the air cooled Zr–1.5Nb–0.4Sn–0.2Fe–0.1Cr alloy has more irregular metal/oxide interfaces, although the air cooled Zr–1.5Nb–0.4Sn–0.2Fe–0.1Cr alloy has a better corrosion

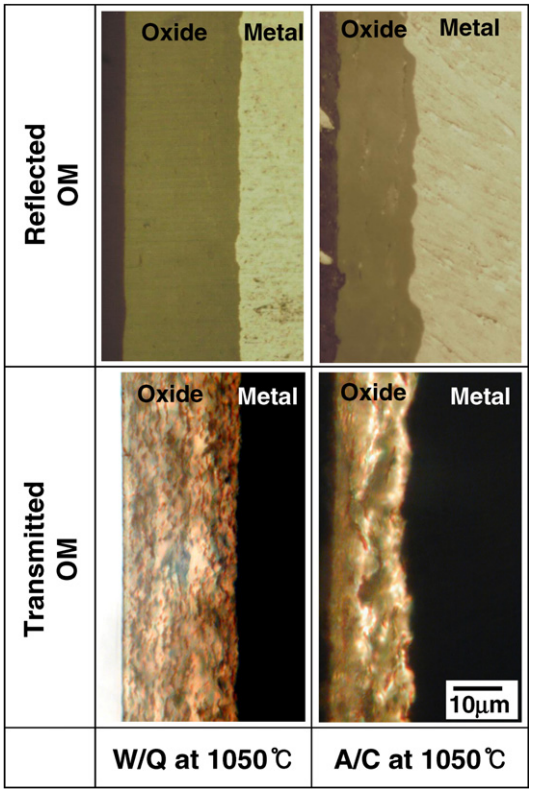

Fig. 6. Reflected and transmitted optical micrographs of the oxide formed on the Zr–1.5Nb–0.4Sn–0.2Fe–0.1Cr alloy with different cooling rates.

resistance than the water quenched alloy. It may be caused by the matrix homogeneity of the alloying element. From the inhomogeneity of the alloying element between the α-phase and the β-phase, the corrosion rate was differently in a local area. Therefore, irregular metal/oxide interfaces were formed in the air cooled Zr–1.5Nb–0.4Sn–0.2Fe–0.1Cr alloy. But the corrosion resistance of the Zr–1.5Nb–0.4Sn–0.2Fe–0.1Cr alloy was increased by an air cooling from the β-region, because the oxide thickness of the air cooled Zr–1.5Nb–0.4Sn–0.2Fe–0.1Cr alloy was thinner than that of the water quenched Zr–1.5Nb–0.4Sn–0.2Fe–0.1Cr alloy.

A cross-sectional oxide layer examined by a transmitted optical microscope was reported by A. Yilmazbayhan et al. [22]. From the information of the transmitted optical microscope, they found that the formation of a periodic layered structure was related to the transition behavior and the dark bands were interpreted as an increased density of smaller the grains and possible cracks. Since the optical light of microscopy could be transmitted for the thin oxide film, the layer structure in the oxide, which is closely related to the changes of the grain morphology, revealed by using the transmitted optical microscopy. The transmitted light could have been more scattered in the small size equiaxed grains compared to the columnar grains. This implies that the difference of contrast in oxide microscopy is caused by the change of the oxide morphology during the oxide grows.

The layered structure in the cross-sectional oxide of the β-annealed Zr–1.5Nb–0.4Sn–0.2Fe–0.1Cr alloy was not observed clearly. However, very small dark lines were randomly distributed in the oxide of the water quenched Zr–1.5Nb–0.4Sn–0.2Fe–0.1Cr alloy and some large dark bands were observed in the oxide of air cooled that alloy. In the view point of correlation between layered structure and transition behavior of corrosion, the transition point could be estimated from the layered structure. Since, the layered structure was not clearly observed in the oxide of the β-annealed Zr–1.5Nb–0.4Sn–0.2Fe–0.1Cr alloy, it could be assumed that the transition of corrosion rate was not was not observed in the β-annealed Zr–1.5Nb–0.4Sn–0.2Fe–0.1Cr alloy as shown in Fig. 5. From the results of the transmitted optical microscopy in this study, it was assumed that the corrosion rate was related to the size and density of the dark lines in the oxides, because the size and density of dark lines in the cross-sectional oxide micrograph was changed with the different corrosion rates which were shown in the water quenched and air cooled Zr–1.5Nb–0.4Sn–0.2Fe–0.1Cr alloy.

From the TEM observation, the oxide characteristics such as grain morphology, cracks, and precipitate dissolution could be identified. Since, the formation of cracks and the a lot of volume fractions of equiaxed grains in the oxide layer was increased of a diffusion path of oxygen ions, the corrosion behavior of zirconium alloys could be assumed from the microstructure characteristics obtained by TEM techniques. Fig. 7 shows the cross-sectional TEM oxide micrographs of the water quenched and air cooled Zr–1.5Nb–0.4Sn–0.2Fe–0.1Cr alloys which were corroded for 60 days. Although the oxide thickness of both alloys was different, it could be observed that the oxide morphology characteristics were changed with the oxide depth. At the same position of the oxide depth such as the metal/oxide interfaces (A), middle oxide layer (B), and outer oxide layer (C), a columnar oxide was developed well in the case of the air cooled Zr–1.5Nb–0.4Sn–0.2Fe–0.1Cr alloy when compared to that of the water quenched Zr–1.5Nb–0.4Sn–0.2Fe–0.1Cr alloy. A correlation between the oxide microstructure and the corrosion behavior of the Nb-containing Zr alloys has been reported [20]. From this result, the better corrosion resistance of the air cooled Zr–1.5Nb–0.4Sn–0.2Fe–0.1Cr alloy resulted from a columnar shape oxide formation and an inhibition of a crack formation in the oxide layer. Based on a previous study [20], the oxide characteristics were mainly controlled by the supersaturated Nb content in the matrix which was determined by the heat-treatment conditions.

From a study of the microstructural characteristics and corrosion behavior of the Zr–1.5Nb–0.4Sn–0.2Fe–0.1Cr alloy with a β-annealing, the corrosion resistance of this alloy was increased by applying a slow cooling rate, however, it is considered to be from a inhomogeneity of the alloying element as a result of a formation of a lamellar shape of the β-Zr in the matrix by a slow cooling. It is possible that the corrosion resistance could be improved by

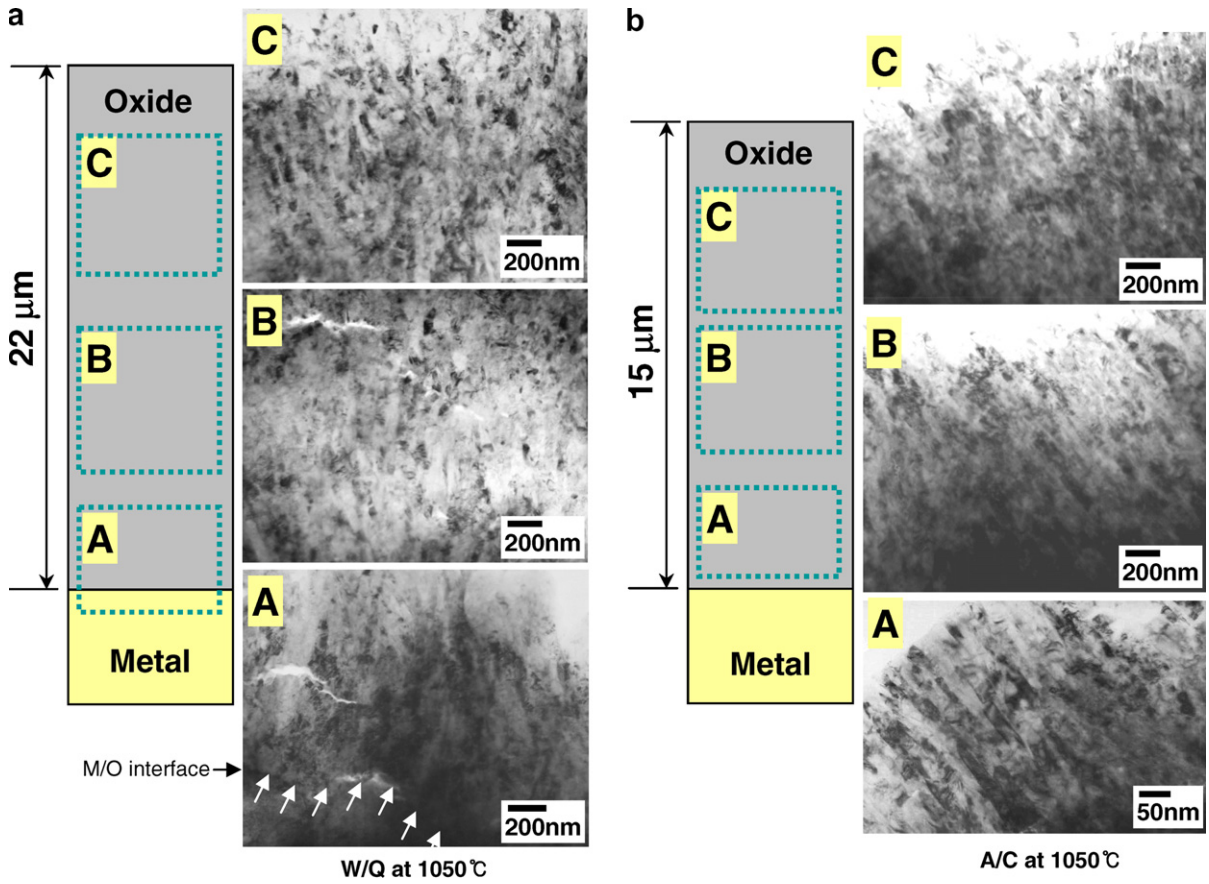

Fig. 7. Cross-sectional TEM oxide morphology formed on the Zr–1.5Nb–0.4Sn–0.2Fe–0.1Cr alloy with different cooling rates.

controlling the intermediate heat-treatment process during the manufacturing process after a β-solution annealing. On the contrary, the β-Zr phase with a lamellar shape was not easily removed by the intermediate heat-treatment process except for a β-solution annealing. Therefore, it is considered that a fast cooling rate after a β-solution annealing should be applied for the Zr–1.5Nb–0.4Sn–0.2Fe–0.1Cr alloy to obtain a good homogeneity of the alloying elements. Also, the β-annealing temperature of this alloy could be determined by this study because it was revealed that the $\alpha+\beta$ to β transition temperature of the Zr–1.5Nb–0.4Sn–0.2Fe–0.1Cr alloy was lower than 960 °C.

4. Conclusion

From the results of the microstructural observations and the corrosion tests for the Zr–1.5Nb–0.4Sn–0.2Fe–0.1Cr alloy, it was revealed that the $\alpha+\beta$ to β transus temperature of that alloy was lower than 960 °C. And a martensite structure was formed by a water quenching and a Widmanstätten structure containing a lamellar shape of the β-Zr phase was formed by an air cooling. The corrosion resistance of the Zr–1.5Nb–0.4Sn–0.2Fe–0.1Cr alloy was not affected by the different β-annealing temperatures of 960, 1050, and 1200 °C, however, the corrosion resistance of this alloy was increased by a slow cooling when compared to a fast cooling. Although the corrosion behavior was improved by applying a slow cooling, a good homogeneity could not obtained by a slow cooling condition. Therefore, it is concluded that a fast cooling rate after a β-solution annealing should be applied to the Zr–1.5Nb–0.4Sn–0.2Fe–0.1Cr alloy to obtain a good homogeneity of the alloying element.

Acknowledgements

This study was supported by Korea Institute of Science and Technology Evaluation and Planning (KISTEP) and Ministry of Science and Technology (MOST), Korean government, through its National Nuclear Technology Program.

References

[1] A.V. Nikulina, J. Nucl. Mater. 238 (1996) 205.
[2] R.J. Comstock, G. Schoenberger, G.P. Sabol, ASTM STP 1295 (1996) 710.
[3] Y.H. Jeong, H.G. Kim, T.H. Kim, J. Nucl. Mater. 317 (2003) 1.
[4] C.M. Eucken, P.T. Finden, S. Trapp-Pritsching, H.G. Weidinger, ASTM STP 1023 (1989) 113.
[5] F. Garzarolli, H. Stehle, E. Steinberg, ASTM STP 1295 (1996) 12.
[6] K. Takeda, H. Anada, ASTM STP 1354 (2000) 592.
[7] Z. NishiyamaMartensite Transformation, vol. 6, Academic Press, New York, 1978.

[8] D.A. Porter, K.E. Resterling, Phase Transformation in Materials (1997) 424.
[9] C.M. Weyman, Solid to Solid Transformation (1982) 1120.
[10] Z. Nishiyama, Martensitic Transformation (1978) 74.
[11] G. Okvist, K. Kallstrom, J. Nucl. Mater. 35 (1970) 316.
[12] O.T. Woo, K. Tangri, J. Nucl. Mater. 79 (1979) 82.
[13] C.D. Williams, R.W. Gilbert, Trans. Jpn. Inst. Met. 9 (Suppl.) (1968) 625.
[14] B.K. Choi, H.G. Kim, Y.H. Jeong, J. Korean Soc. Heat Treatment 17 (5) (2004) 271.
[15] R.A. Holt, J. Nucl. Mater. 35 (1970) 322.
[16] H.M. Chung, T.F. Kassner, J. Nucl. Mater. 84 (1979) 327.
[17] D.O. Northwood, D.T. Lim, Can. Metall. Quart. 18 (1979) 441.
[18] B.K. Choi, H.G. Kim, Y.H. Jeong, J. Korean Soc. Heat Treatment 17 (5) (2004) 271.
[19] Y.H. Jeong, K.O. Lee, H.G. Kim, J. Nucl. Mater. 302 (2002) 9.
[20] Y.H. Jeong, H.G. Kim, T.H. Kim, J. Nucl. Mater. 317 (2003) 1.
[21] H.G. Kim, Y.H. Jeong, T.H. Kim, J. Nucl. Mater. 326 (2004) 125.
[22] A. Yilmazbayhan, A.T. Motta, R.J. Comstock, G.P. Sabol, B. Lai, Z. Cai, J. Nucl. Mater. 324 (2004) 6.